Improved effective-bond-orbital model for superlattices

John P. Loehr
Solid State Electronics Directorate (WL/ELRA), Wright-Patterson Air Force Base, Dayton, Ohio 45433-6543
(Received 27 December 1993; revised manuscript received 22 April 1994)

We have augmented the effective-bond-orbital model to include second-nearest-neighbor overlap integrals. With these additional parameters we can fit the band energies at the Γ *and* X points, in addition to the zero-center masses. This model provides a more accurate bulk band structure with a negligible increase in computation time. The improved model is applied to short-period type-II InAs/$In_xGa_{1-x}Sb$ superlattices, and we observe a significant departure from the nearest-neighbor results.

I. INTRODUCTION

Superlattice band-structure calculations comprise a topic of perennial interest to solid-state and device physicists. Currently, there are many methods that can generate reasonable results. In general, though, to obtain increased accuracy one must drastically escalate the computation time for a given algorithm. The most computationally benign—if not the most accurate—schemes are usually based upon atomic orbitals or, equivalently, zone-center basis functions. The $\mathbf{k}\cdot\mathbf{p}$ method[1,2] can accurately describe a few bands near the zone center, in the sense that the zone-center band gaps and second-order band dispersions will be correct. Depending upon the accuracy required and the energy range of interest, various numbers of bands may be included. To describe free-carrier states and optical absorption, one is typically interested in only the conduction, heavy, light, and split-off bands. When the spin degeneracy is included, this results in an 8×8 $\mathbf{k}\cdot\mathbf{p}$ Hamiltonian. Of course, this description is only strictly valid near the zone center; more bands are required to describe states with large crystal momentum $\mathbf{k}$ or extreme energy. In bulk material, additional bands may be easily accommodated. In superlattices, however, the resulting system of coupled differential equations is often solved by a direct matrix approach.[3] In this case, adding even a few extra bands will rapidly increase the dimensionality of the matrix. Since the diagonalization time of an $N\times N$ matrix grows as N^3, this can dramatically extend the computation time. It is clear, then, that if we want to improve the range or accuracy of the model, we are better off refining the 8×8 matrix than adding more bands.

In this respect, the effective-bond-orbital model (EBOM) is a step in the right direction.[4] Here instead of taking a perturbation-theory approach, the semiconductor bands are described by a face-centered-cubic (fcc) tight-binding Hamiltonian. In order to calculate the conduction, heavy, light, and split-off bands of either spin, one includes spin-doubled s,p_x,p_y,p_z orbitals to generate an 8×8 Hamiltonian. The parameters are determined by fitting the band gap, the split-off gap, and the zone-center mass of each band. Additionally, the heavy- and light-hole splitting at the X point is constrained. This provides a tight-binding matrix whose small-$\mathbf{k}$ expansion returns exactly the 8×8 $\mathbf{k}\cdot\mathbf{p}$ Hamiltonian. One advantage of the EBOM technique is that it is often easier to implement the tight-binding superlattice-slab matrix[5] than it is to solve the coupled system of differential equations resulting from the $\mathbf{k}\cdot\mathbf{p}$ method—especially with regard to the interfacial boundary conditions. Perhaps a more significant advantage is that the fcc tight-binding method is in principle valid throughout the zone. In particular, it should be more accurate than the $\mathbf{k}\cdot\mathbf{p}$ method for larger $\mathbf{k}$. Since the band structure of short-period superlattices will sample large-$\mathbf{k}$ states from the growth direction, we may expect the EBOM to be more accurate for thin-layer structures. Of course, the more complete sp^3s^* zinc-blende empirical-tight-binding model[6] (ETBM) can be expected to give even greater accuracy, but this model requires that we again include bands with which we are unconcerned (the higher conduction bands and lower valence bands) in order to get a more accurate answer near the band gap. Also, it can be difficult to determine the parameters for this model, especially if we want to fit the effective masses as well as the Γ, X, and L gaps.

Thus, it seems that the EBOM can provide an excellent superlattice description on a price and/or performance measure. This is especially true in narrow band-gap or type-II superlattices where the conduction-band–valence-band coupling is significant. In this paper, we make a simple improvement to the model that will enhance its accuracy for short-period (001) superlattices with only a small increase in cost. By adding second-nearest neighbors to the model, we can fit all of the zone-center masses, the Γ-point gaps, *and* the X gaps as well. We present this modification in Sec. II and conclude with the results in Sec. III.

II. INCLUSION OF SECOND-NEAREST NEIGHBORS

We are interested in the energy band structure of compound semiconductors. These typically form into a zinc-blende crystal structure consisting of a two-atom anion-cation *basis* that is repeated on each site of a face-centered-cubic *lattice*. Rather than specializing our tight-binding model to the *crystal* structure,[6] we take the EBOM approach and consider instead only the *lattice* structure.[4] Thus, we assume a set of "effective" orbitals $\phi_\alpha(\mathbf{r}-\mathbf{R})$ localized on the fcc lattice sites $\mathbf{R}$ of the zinc-

blende crystal. We form a trial wave function $\Psi_k(\mathbf{r})$ by taking a linear combination of Bloch sums of these orbitals, i.e.,

$$\Psi_{\mathbf{k}}(\mathbf{r})=\frac{1}{\sqrt{N}}\sum_{\alpha}c_{\alpha}(\mathbf{k})\sum_{\mathbf{R}}e^{i\mathbf{k}\cdot\mathbf{R}}\phi_{\alpha}(\mathbf{r}-\mathbf{R})\ , \tag{1}$$

where N represents the number of lattice sites in the crystal. Upon substituting this wave function into the Schrödinger equation $H\Psi=E\Psi$, we obtain the tight-binding secular equation. Since we have explicitly included the Bloch phases $e^{i\mathbf{k}\cdot\mathbf{R}}$ at each lattice site, the secular equation is diagonal in $\mathbf{k}$. We are only concerned with the conduction and valence bands near the band gap, and so we consider only orbitals ϕ_α that transform under elements of the fcc point group like s and p states. If we direct the p orbitals along the crystal axes x, y, and z we get the 4×4 secular equation

$$\begin{bmatrix} \langle s|H|s\rangle & \langle s|H|p_x\rangle & \langle s|H|p_y\rangle & \langle s|H|p_z\rangle \\ \langle p_x|H|s\rangle & \langle p_x|H|p_x\rangle & \langle p_x|H|p_y\rangle & \langle p_x|H|p_z\rangle \\ \langle p_y|H|s\rangle & \langle p_y|H|p_x\rangle & \langle p_y|H|p_y\rangle & \langle p_y|H|p_z\rangle \\ \langle p_z|H|s\rangle & \langle p_z|H|p_x\rangle & \langle p_z|H|p_y\rangle & \langle p_z|H|p_z\rangle \end{bmatrix} \begin{bmatrix} c_s(\mathbf{k}) \\ c_{p_x}(\mathbf{k}) \\ c_{p_y}(\mathbf{k}) \\ c_{p_z}(\mathbf{k}) \end{bmatrix} = E(\mathbf{k}) \begin{bmatrix} c_s(\mathbf{k}) \\ c_{p_x}(\mathbf{k}) \\ c_{p_y}(\mathbf{k}) \\ c_{p_z}(\mathbf{k}) \end{bmatrix} . \tag{2}$$

We now evaluate each matrix element by taking the sum over $\mathbf{R}$ in Eq. (1) up to *second*-nearest neighbors. If we assume that the *conventional* fcc unit cell has lattice constant a (i.e., $a=5.65$ Å for GaAs) then the elements are[7]

$$\begin{aligned}\langle s|H|s\rangle =& E_{ss}(000)\\ &+4E_{ss}(110)[\cos\xi\cos\eta+\cos\eta\cos\rho+\cos\xi\cos\rho]\\ &+2E_{ss}(200)[\cos(2\xi)+\cos(2\eta)+\cos(2\rho)]\ ,\end{aligned} \tag{3}$$

$$\langle s|H|p_x\rangle =4iE_{sx}(110)\sin\xi[\cos\eta+\cos\rho] +2iE_{sx}(200)\sin(2\xi)\ , \tag{4}$$

$$\begin{aligned}\langle p_x|H|p_x\rangle =& E_{xx}(000)+4E_{xx}(110)\cos\xi[\cos\eta+\cos\rho]\\ &+4E_{xx}(011)\cos\eta\cos\rho+2E_{xx}(200)\cos(2\xi)\\ &+2E_{xx}(002)[\cos(2\eta)+\cos(2\rho)]\ ,\end{aligned} \tag{5}$$

$$\langle p_x|H|p_y\rangle =-4E_{xy}(110)\sin\xi\sin\eta\ . \tag{6}$$

Here $\xi=k_xa/2$, $\eta=k_ya/2$, $\rho=k_za/2$, and the other elements are obtained by cyclic permutation.

In any tight-binding Hamiltonian, we may choose to include either two-center or three-center integrals. Typically there are more three-center than two-center orbitals; thus, the three-center approach supplies more disposable constants. The original nearest-neighbor EBOM (Ref. 4) was written with three-center integrals, providing enough parameters to fit the zone-center masses and the Γ-point gaps. With our second-nearest neighbors, though, we will already have enough two-center integral parameters to satisfy all of our constraints. Hence, we find it more convenient to write the three-center matrix elements above as the following linear combinations of two-center integrals:

$$E_{ss}(000)=V_{ss0}\ , \tag{7}$$

$$E_{ss}(110)=V_{ss1}\ , \tag{8}$$

$$E_{ss}(200)=V_{ss2}\ , \tag{9}$$

$$E_{sx}(110)=V_{sp1}\ , \tag{10}$$

$$E_{sx}(200)=V_{sp2}\ , \tag{11}$$

$$E_{xx}(000)=V_{pp0}\ , \tag{12}$$

$$E_{xx}(110)=\tfrac{1}{2}V^{\sigma}_{pp1}+\tfrac{1}{2}V^{\pi}_{pp1}\ , \tag{13}$$

$$E_{xx}(011)=V^{\pi}_{pp1}\ , \tag{14}$$

$$E_{xx}(200)=V^{\sigma}_{pp2}\ , \tag{15}$$

$$E_{xx}(002)=V^{\pi}_{pp2}\ , \tag{16}$$

$$E_{xy}(110)=\tfrac{1}{2}V^{\sigma}_{pp1}-\tfrac{1}{2}V^{\pi}_{pp1}\ . \tag{17}$$

When we develop constraint equations to fix these two-center integrals, we will find that even by fitting the masses of each bond at the Γ point ($\xi=\eta=\rho=0$) and the energies of each band at the X ($\xi=\pi,\eta=\rho=0$) and Γ points, we cannot uniquely separate V_{sp1} and V_{sp2}. Therefore, we include only the nearest-neighbor sp matrix element (V_{sp1}), leaving us with the nine independent parameters V_{ss0}, V_{ss1}, V_{ss2}, V_{sp1}, V_{pp0}, V^{σ}_{pp1}, V^{π}_{pp1}, V^{σ}_{pp2}, and V^{π}_{pp2}. We will choose these by fitting the conduction-band (E_c) and valence-band (E_v) energies at the Γ point (two constraints), the conduction-band (X_{1c}), doubly degenerate valence-band (X_{5v}), and nondegenerate valence-band (X_{3v}) energies at the X point (three constraints), and the conduction, heavy, light, and split-off masses at Γ (four constraints).[9]

By solving the matrix equation (2) we can easily obtain the Γ-point energies

$$E_c=V_{ss0}+12V_{ss1}+6V_{ss2}\ \text{(nondegenerate)}\ , \tag{18}$$

$$E'_v=V_{pp0}+4V^{\sigma}_{pp1}+8V^{\pi}_{pp1} +2V^{\sigma}_{pp2}+4V^{\pi}_{pp2}\ \text{(triply degenerate)}\ , \tag{19}$$

and the X-point energies

$$X_{1c}=V_{ss0}-4V_{ss1}+6V_{ss2}\ \text{(nondegenerate)}\ , \tag{20}$$

$$X_{5v}=V_{pp0}-4V^{\pi}_{pp1}+2V^{\sigma}_{pp2}+4V^{\pi}_{pp2}\ \text{(doubly degenerate)}\ , \tag{21}$$

$$X_{3v}=V_{pp0}-4V_{pp1}^{\sigma}+2V_{pp2}^{\sigma}+4V_{pp2}^{\pi} \quad \text{(nondegenerate)} . \tag{22}$$

Here we have written the valence-band-edge energy as E_v' instead of E_v in anticipation of the spin-orbit corrections to follow.

Next we must calculate the Γ-point masses in our model and fit them to experiment. For this, we Taylor expand the matrix in Eq. (2) about $\mathbf{k}=0$. Since the form of this expansion is set by the fcc lattice symmetry, and not by the number of neighbors included, we still obtain the same matrix form as in Ref. 4,

$$H_{\mathbf{k}\cdot\mathbf{p}}=\begin{bmatrix} E_c-\nu_1 k^2 & 4iV_{sp}ak_x & 4iV_{sp}ak_y & 4iV_{sp}ak_z \\ -4iV_{sp}ak_x & E_v'-\lambda_1 k_x^2-\lambda_2 k^2 & -\lambda_3 k_x k_y & -\lambda_3 k_x k_z \\ -4iV_{sp}ak_y & -\lambda_3 k_x k_y & E_v'-\lambda_1 k_y^2-\lambda_2 k^2 & -\lambda_3 k_y k_z \\ -4iV_{sp}ak_z & -\lambda_3 k_x k_z & -\lambda_3 k_y k_z & E_v'-\lambda_1 k_z^2-\lambda_2 k^2 \end{bmatrix} . \tag{23}$$

The difference is that our coefficients now include *second*-neighbor integrals as well, giving[8]

$$\nu_1=(V_{ss1}+V_{ss2})a^2 , \tag{24}$$

$$\lambda_1=(V_{pp1}^{\sigma}-V_{pp1}^{\pi}+4V_{pp2}^{\sigma}-4V_{pp2}^{\pi})a^2/4 , \tag{25}$$

$$\lambda_2=(V_{pp1}^{\sigma}+3V_{pp1}^{\pi}+4V_{pp2}^{\pi})a^2/4 , \tag{26}$$

$$\lambda_3=(V_{pp1}^{\sigma}-V_{pp1}^{\pi})a^2/2 . \tag{27}$$

Of course, this is exactly the same form as the sp^3 $\mathbf{k}\cdot\mathbf{p}$ Hamiltonian in the absence of spin-orbit coupling,[2] since that matrix is also determined from the fcc lattice symmetry.

To describe the bands near Γ, it is essential to include spin-orbit effects into the model. Here we follow the usual practice by doubling the basis set from sp^3 to $s\uparrow, p_x\uparrow, p_y\uparrow, p_z\uparrow, s\downarrow, p_x\downarrow, p_y\downarrow, p_z\downarrow$ and by coupling the spin and orbital parts to total angular momentum states $|j,m\rangle$ through the Clebsch-Gordan coefficients.[10] We then treat the spin-orbit coupling phenomenologically by adding a spin-orbit Hamiltonian that acts upon the $|j,m\rangle$ states as $H_{\text{s.o.}}=(2\Delta/3\hbar^2)\mathbf{L}\cdot\mathbf{S}$. This form is chosen to reproduce the split-off gap Δ when evaluated in the $sp^3\times(\uparrow,\downarrow)$ basis. Since this term actually raises the $j=\frac{3}{2}$ states by $\Delta/3$ and lowers the $j=\frac{1}{2}$ states by $2\Delta/3$ we must correct the valence-band edge, and so we have used $E_v'\equiv E_v-\Delta/3$ in Eq. (19).

Of course, the spin-orbit coupling will also influence the X-point energies (20)–(22). Specifically, the X_{1c} state is unchanged and one of the degenerate X_{5v} states is shifted upward by $\Delta/3$; the other X_{5v} state and the X_{3v} state emerge as the surd-pair roots of a quadratic equation and so cannot be treated conveniently. These roots remain very close to the $\Delta=0$ values. In GaAs, for example, the spin-orbit term shifts the X_{5v} state downward by 108 meV and shifts the X_{3v} state upward by 6 meV. Since these shifts are small in magnitude compared to the X-point energies themselves, we neglect X-point spin corrections in favor of maintaining our linear equations (20)–(22).

It is convenient to have the matrix elements of $H_{\text{s.o.}}$ in the $(sp^3)\times(\uparrow,\downarrow)$ basis. If we quantize our angular momenta about the z axis and respect the standard Condon-Shortley phases, we obtain the nonzero matrix elements

$$\begin{aligned}
&\langle p_x\uparrow|H_{\text{s.o.}}|p_y\uparrow\rangle=-\frac{i\Delta}{3}=\langle p_y\uparrow|H_{\text{s.o.}}|p_x\uparrow\rangle^* , \\
&\langle p_x\uparrow|H_{\text{s.o.}}|p_z\downarrow\rangle=\frac{\Delta}{3}=\langle p_z\downarrow|H_{\text{s.o.}}|p_x\uparrow\rangle , \\
&\langle p_y\uparrow|H_{\text{s.o.}}|p_z\downarrow\rangle=-\frac{i\Delta}{3}=\langle p_z\downarrow|H_{\text{s.o.}}|p_y\uparrow\rangle^* , \\
&\langle p_z\uparrow|H_{\text{s.o.}}|p_x\downarrow\rangle=-\frac{\Delta}{3}=\langle p_x\downarrow|H_{\text{s.o.}}|p_z\uparrow\rangle , \\
&\langle p_z\uparrow|H_{\text{s.o.}}|p_y\downarrow\rangle=\frac{i\Delta}{3}=\langle p_y\downarrow|H_{\text{s.o.}}|p_z\uparrow\rangle^* , \\
&\langle p_x\downarrow|H_{\text{s.o.}}|p_y\downarrow\rangle=\frac{i\Delta}{3}=\langle p_y\downarrow|H_{\text{s.o.}}|p_x\downarrow\rangle^* .
\end{aligned} \tag{28}$$

Then in the $(sp^3)\times(\uparrow,\downarrow)$ basis the full 8×8 Hamiltonian is given to second order in $\mathbf{k}$ by

$$H=\begin{bmatrix} H_{\mathbf{k}\cdot\mathbf{p}} & 0 \\ 0 & H_{\mathbf{k}\cdot\mathbf{p}} \end{bmatrix}+[H_{\text{s.o.}}] , \tag{29}$$

where the 4×4 matrix $H_{\mathbf{k}\cdot\mathbf{p}}$ is given in Eq. (23).

If we transform this matrix H to the $|j,m\rangle$ basis with the Clebsch-Gordan coefficients, we can solve for the dispersion by perturbation theory. The conduction (CB), heavy (HH), light (LH), and split-off (SO) bands are then obtained to second order as

$$E_{\text{CB}}(\mathbf{k})=E_g+\left[-\nu_1+\chi a^2\left[1+\frac{r}{2}\right]\right]k^2 , \tag{30}$$

$$\begin{aligned}
E_{LH}^{HH}(\mathbf{k})=E_v-&\left[\frac{\lambda_1}{3}+\lambda_2+\frac{\chi}{2}a^2\right]k^2 \\
&\pm\tfrac{1}{3}[(\lambda_1+\tfrac{3}{2}\chi a^2)^2(k_x^4+k_y^4+k_z^4) \\
&+(-\lambda_1^2+3\lambda_3^2-3\lambda_1\chi a^2+9\lambda_3\chi a^2+\tfrac{9}{2}\chi^2a^4) \\
&\times(k_x^2k_y^2+k_x^2k_z^2+k_y^2k_z^2)]^{1/2} ,
\end{aligned} \tag{31}$$

$$E_{\text{SO}}(\mathbf{k})=E_v-\Delta-\left[\frac{\lambda_1}{3}+\lambda_2+\frac{\chi}{2}a^2r\right]k^2 , \tag{32}$$

where

$$r \equiv \frac{E_g}{E_g+\Delta} , \quad \chi \equiv \frac{2(4V_{sp})^2}{3E_g} , \quad E_g \equiv E_c - E_v . \tag{33}$$

If we compare carefully, we see this is exactly the same form as the second-order solution to the 8×8 $\mathbf{k}\cdot\mathbf{p}$ Hamiltonian,[11] provided that we identify

$$\lambda_1 = 6R_0 a^2 \gamma_2 , \tag{34}$$

$$\lambda_2 = R_0 a^2 (\gamma_1 - 2\gamma_2) , \tag{35}$$

$$\lambda_3 = 6R_0 a^2 \gamma_3 , \tag{36}$$

where

$$R_0 \equiv \frac{\hbar^2}{2m_0 a^2} . \tag{37}$$

Here the γ_i are the "modified" Luttinger parameters that implicitly include the effects of conduction-band–valence-band coupling. It is more common, though, to have empirical access to the "true" Luttinger parameters $\gamma_{j,L}$ in which the interband coupling has been explicitly separated out.[12] The two are related by[11]

$$\gamma_1 \equiv \gamma_{1,L} - \frac{\chi}{2R_0} , \tag{38}$$

$$\gamma_2 \equiv \gamma_{2,L} - \frac{\chi}{4R_0} , \tag{39}$$

$$\gamma_3 \equiv \gamma_{3,L} - \frac{\chi}{4R_0} . \tag{40}$$

Now we can substitute Eqs. (25)–(27) and (38)–(40) into Eqs. (34)–(36), to express the *true* Luttinger parameters in terms of our two-center integrals as

$$24R_0\gamma_{2,L} = V^{\sigma}_{pp1} - V^{\pi}_{pp1} + 4V^{\sigma}_{pp2} - 4V^{\pi}_{pp2} + 6\chi , \tag{41}$$

$$4R_0(\gamma_{1,L} - 2\gamma_{2,L}) = V^{\sigma}_{pp1} + 3V^{\pi}_{pp1} + 4V^{\pi}_{pp2} , \tag{42}$$

$$12R_0\gamma_{3,L} = V^{\sigma}_{pp1} - V^{\pi}_{pp1} + 3\chi . \tag{43}$$

Finally, the conduction-band mass m_c is obtained by taking the k^2 coefficient from Eq. (30) and inserting Eq. (24) to yield

$$R_0\frac{m_0}{m_c} = -V_{ss1} - V_{ss2} + \left[1+\frac{r}{2}\right]\chi . \tag{44}$$

At this point we are essentially done. The nine constraint equations (18)–(22) and (41)–(44) are linear and independent in the nine parameters V_{ss0}, V_{ss1}, V_{ss2}, V_{pp0}, V^{σ}_{pp1}, V^{π}_{pp1}, V^{σ}_{pp2}, V^{π}_{pp2}, and χ. Thus, they may be inverted to obtain the two-center integrals in terms of the empirical parameters via

$$V_{ss0} = (5E_c + 3X_{1c})/8 + 6R_0\frac{m_0}{m_c} + \left[1+\frac{r}{2}\right][(X_{5v} - X_{3v})/2 - 24R_0\gamma_{3,L}] , \tag{45}$$

$$V_{ss1} = (E_c - X_{1c})/16 , \tag{46}$$

$$V_{ss2} = (X_{1c} - E_c)/16 - R_0\frac{m_0}{m_c} + \left[1+\frac{r}{2}\right][(X_{3v} - X_{5v})/12 + 4R_0\gamma_{3,L}] , \tag{47}$$

$$V_{pp0} = (5E'_v + 3X_{3v})/8 - 6R_0(\gamma_{1,L} - 2\gamma_{3,L}) , \tag{48}$$

$$V^{\sigma}_{pp1} = (E'_v - 3X_{3v} + 2X_{5v})/16 , \tag{49}$$

$$V^{\pi}_{pp1} = (E'_v + X_{3v} - 2X_{5v})/16 , \tag{50}$$

$$V^{\sigma}_{pp2} = (2X_{5v} - X_{3v} - E'_v)/16 + R_0(\gamma_{1,L} + 4\gamma_{2,L} - 6\gamma_{3,L}) , \tag{51}$$

$$V^{\pi}_{pp2} = (X_{5v} - E'_v)/16 + R_0(\gamma_{1,L} - 2\gamma_{2,L}) , \tag{52}$$

$$\chi = (X_{3v} - X_{5v})/12 + 4R_0\gamma_{3,L} . \tag{53}$$

Now we can get all of our tight-binding matrix elements by evaluating Eqs. (7)–(17) and (33) with these parameters. This completely determines the second-nearest-neighbor Hamiltonian and assures that the solutions will be fitted to the Γ and X energies, as well as to the zone-center effective masses. It is interesting to note that if we had tried instead to fit the bands to the L-point energies, the constraint equations would *not* have been independent, and so could not have been uniquely inverted.

III. RESULTS AND CONCLUSION

Because of the complex relationships between the input parameters and the calculated bands, it is difficult to make intuitive comparisons between the second-neighbor corrections to the EBOM and the ETBM. In either model, the second-nearest neighbors add higher periodicity terms (in $\mathbf{k}$) to the Hamiltonian, consequently allowing much greater flexibility in the band curvatures. In the EBOM it is quite easy to add second neighbors, since there are only two additional parameters *and* these parameters can be determined directly from the empirical input. In the ETBM, by contrast, the second-neighbor parameters are usually determined by numerical optimization.

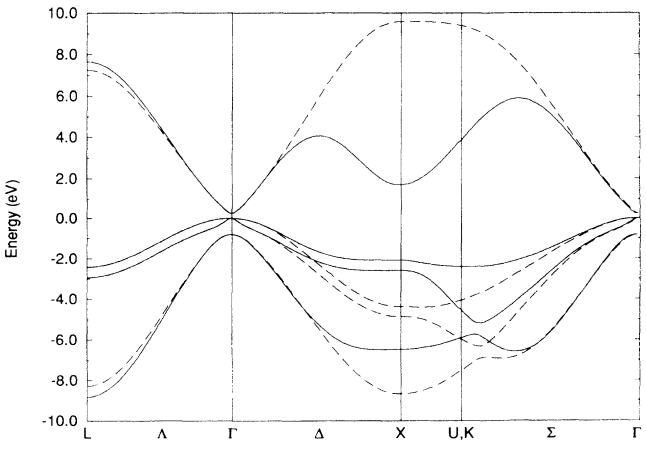

FIG. 1. InSb band structure in the nearest-neighbor (dotted lines) and next-nearest-neighbor (solid lines) EBOM.

We illustrate the difference between the nearest-neighbor and the second-nearest-neighbor EBOM in Fig. 1, where we show the InSb band structure for both models. Although they give identical results near Γ, we see dramatic differences at the X point. We also remark that the X and L point behavior of the nearest-neighbor EBOM can be very sensitive to the conduction-band mass: for some values of m_c, the X and L conduction-band energies may dip below E_c, making the model unsuitable for superlattice calculations. For example, the GaSb material parameters are often given as $\gamma_{1,L}=11.89$, $\gamma_{2,L}=4.92$, $\gamma_{3,L}=5.19$, $\Delta=0.77$, $E_g=0.81$, $a=6.0959$, and $m_c/m_0=0.042$. These produce an erroneous conduction band in the nearest-neighbor EBOM; if we set $m_c/m_0=0.045$, the bands are reasonable. Of course, one could reverse the interpretation and argue that the former parameter set is, in fact, not physically acceptable. In any event, the second-neighbor EBOM is much less sensitive to the bulk material parameters and will work with either parameter set.

The X-point difference between the models can cause striking differences in the superlattice energies, especially for short-period type-II superlattices where the wave functions are quite likely to sample the X-point bulk behavior. In Fig. 2, we show the band gaps for an $(InAs)_n/(In_xGa_{1-x}Sb)_n$ superlattice grown on a GaSb substrate as a function of the monolayer number n for various x values. The bands were calculated by evaluating the slab matrices for the two EBOM Hamiltonians.[5] We obtained the two-center integral parameters for the ternary $In_xGa_{1-x}Sb$ alloy by directly averaging the binary values and we treated strain effects with the deformation-potential theory. All empirical parameters chosen for the bulk materials are given in Ref. 13.

The differences in Fig. 2 are significant at small n, especially for extremal x values. Clearly the bulk X-point behavior of each constituent material can be important in the superlattice description. Comparing our results to 8×8 $\mathbf{k}\cdot\mathbf{p}$ calculations for this system,[14] we see that both EBOM calculations agree favorably, but the *nearest*-neighbor EBOM tracks more closely. This could be anticipated, since the $\mathbf{k}\cdot\mathbf{p}$ model contains no X-point information. Indeed, while the 8×8 $\mathbf{k}\cdot\mathbf{p}$ model agrees completely with both EBOM calculations at Γ, it is grossly

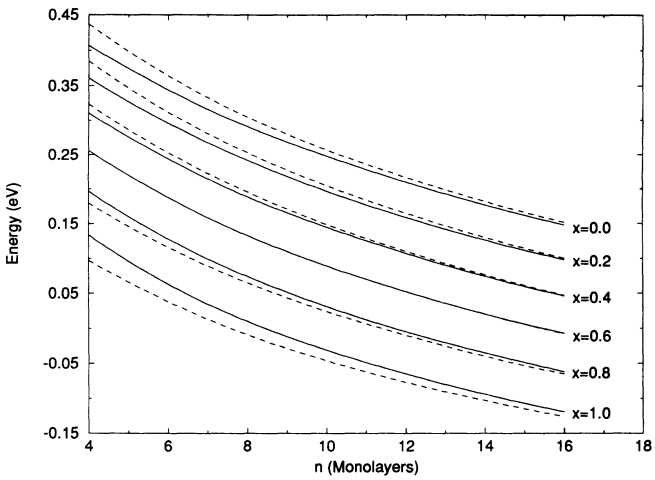

FIG. 2. Band-gap energies for an $(InAs)_n/(In_xGa_{1-x}Sb)_n$ superlattice grown on GaSb in the nearest-neighbor (dotted lines) and next-nearest-neighbor (solid lines) EBOM.

invalid at the X point. This absence of X-point data may compromise the accuracy of $\mathbf{k}\cdot\mathbf{p}$ treatments of very short-period structures. Of course, no model is guaranteed to agree exactly with experiment, but because of the embedded X-point information it is likely that the second-neighbor EBOM will give more accurate results. Additionally, we emphasize that the Luttinger parameters and conduction-band mass must be carefully chosen for each material.

In conclusion, we find that by including *second*-nearest neighbors into the fcc tight-binding framework we can fit the X-point energies as well as the zone-center masses and gaps. This marginally increases the computation time for (001) superlattices, but gives significantly different, and presumably more accurate, results.

ACKNOWLEDGMENT

The author is indebted to Dr. R. E. Sherriff of Wright Laboratory for several critical readings of the manuscript.

[1]J. M. Luttinger and W. Kohn, Phys. Rev. **97**, 869 (1955).
[2]E. O. Kane, *Physics of III-V Compounds* (Academic, New York, 1966), Vol. 1, Chap. 3, pp. 75–100.
[3]D. Ahn, S. L. Chuang, and Y. C. Chang, J. Appl. Phys. **64**, 4056 (1988).
[4]Y. C. Chang, Phys. Rev. B **37**, 8215 (1988).
[5]J. N. Schulman and T. C. McGill, Phys. Rev. Lett. **39**, 1680 (1977).
[6]J. N. Schulman and Y. C. Chang, Phys. Rev. B **31**, 2056 (1985); **31**, 2069 (1985).
[7]J. C. Slater and G. F. Koster, Phys. Rev. **94**, 1498 (1954).
[8]Actually, Eq. (3′) of Ref. 4 should read $E_v=E_p+8E_{xx}+4E_{zz}$, $\lambda_1=(E_{xx}-E_{zz})a^2/2$, and $\lambda_2=(E_{xx}+E_{zz})a^2/2$.
[9]Note that the indicated degeneracies occur only in the absence of spin-orbit effects. Even though we *will* include such effects, we retain this labeling for notational convenience.
[10]Of course, these linear combinations only transform like the total angular momentum states $|j,m\rangle$ under symmetry operations of the fcc point group.
[11]See, for example, R. Eppenga, M. F. H. Schuurmans, and S. Colak, Phys. Rev. B **36**, 1554 (1987) for a description of the 8×8 $\mathbf{k}\cdot\mathbf{p}$ Hamiltonian and its second-order solution. Note also that our parameters χ and R_0 are related to their λ parameter by $R_0\lambda=\chi$.

[12]See, P. Lawaetz, Phys. Rev. B **4**, 3460 (1971) for an oft-cited list of the "true" Luttinger parameters.

[13]D. N. Talwar, J. P. Loehr, and B. Jogai, Phys. Rev. B **49**, 10 345 (1994).

[14]See, for example, C. Mailhiot and D. L. Smith, J. Vac. Sci. Technol. B **5**, 1268 (1987) for calculations of *free-standing* $(InAs)(In_xGa_{1-x}Sb)_n$ superlattices. The results in Fig. 2, by contrast, are for structures lattice matched to a GaSb substrate.